Revue des Energies Renouvelables Vol. 17 N°1 (2014) 55 – 69
DOI: https://doi.org/10.54966/jreen.v17i1.423

Control of a wind energy conversion system based on brushless doubly fed induction generator

Zoheir Tir [1*] and Rachid Abdessemed [2†]

[1] Faculté des Sciences et de Technologie
Université d'El Oued, B.P. 789, 39000, El Oued, Algeria
[2] LEB – Research Laboratory, Dept. Electrical Engineering
Université de Batna, 05000 Batna, Algeria

(reçu le 30 Octobre 2012 - accepté le 30 Mars 2014)

Abstract – *This paper discusses the control a new topology of a brushless doubly-fed induction generator (BDFIG) using back-to-back PWM converters. The goal of BDFIG control is to achieve a similar dynamic performance to the doubly fed induction generator (DFIG), The control strategy for flexible power flow control is developed. Currently the BDFIG has been the subject of current investigation and it shows to be a valid alternative for wind energy systems.*

Résumé - *Cet article discute de la commande d'une nouvelle topologie d'un générateur à induction à double aimantation sans bague balais (BDFIG) en utilisant un convertisseur (AC-AC) bidirectionnel à commande MLI. Le but du contrôle BDFIG est de réaliser une performance dynamique similaire à la génératrice asynchrone à double alimentation (MADA), on a développé une stratégie de commande pour contrôler l'écoulement des puissances. Actuellement, le BDFIG a fait l'objet de l'enquête en cours et il se révèle être une alternative solution pour les systèmes d'énergie éolienne.*

Keywords: Brushless doubly-fed induction generator - d-q vector control – Modeling - PID controller - Wind energy systems - Simulation.

1. INTRODUCTION

The BDFIG is a possible alternative to the conventional doubly fed induction machine (DFIG) [2-11]. Recently the DFIG became the popular configuration in variable speed wind energy applications [1]. The development and use of the DFIG machines was dictated by the need for wide operational range as well as the necessity to allow flexible power flow control, grid integration as well as economic reasons [2-4].

The use of the DFIG machines, however, increased the long term cost and complexity of the wind energy generation. The disadvantage associated with the wound-rotor induction machines is that the slip rings and carbon brushes have to be systematically maintained [3, 6].

Typical faults of slip rings and brushes are: the increased surface roughness of the rings or the brush contact face, break out of carbon material from the brushes and decreasing contact pressing forces which lead to increased brush sparking and significant performance deterioration [7].

* tir-zoheir@univ-eloued.dz
† r.abdessemed@lycos.com

Since wind turbines are installed in remote places, the maintenance costs for such remote installations are significant, [6]. The cost of maintenance for traditional DFIG based wind generators increased the pressure to seek other alternative generator systems [1]. One of such alternatives is offered by the BDFIG as shown in Fig. 1 [2-11].

This type of machine was developed by R. Epée and A. Wallace, of Oregon State University (USA). Currently R.A. McMahon of the University of Combridge (UK) and P.C. Roberts of Scientific Generics Ltd. (UK) work on the analysis of the machine operation and the design of different rotor structures [12].

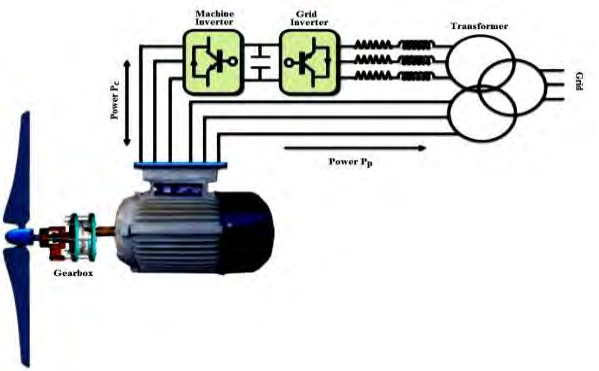

Fig. 1: BDFIG configuration for wind power generation

2. MODELLING OF THE WIND TURBINE AND GEARBOX

The theoretical power available in the wind is defined by Betz formula. It is given by,

$$P_w = \frac{1}{2} \times \rho \times S \times v_w^3 \tag{1}$$

All this power is not recovered on the shaft of the turbine depending on the geometry of the turbine and frictions.

The capture of the wind energy, in an efficient way, requires the existence of a constant wind flow sufficiently strong [13].

Currently wind turbines are designed to achieve a maximum power at wind speeds above 12 m/s.

However, they can be adjusted to the local wind profile.

The maximum theoretical efficiency for the wind to energy conversion is 59.3 % (Betz's Limit). The effective efficiency conversion is given by the power coefficient C_p, which is expressed by the following,

$$C_p = P_t \ / \ P_w \tag{2}$$

The (per unit) speed or relative λ is the ratio between the linear blade speed and the speed of the wind.

$$\lambda = \frac{\Omega_t \times R}{v_w} \tag{3}$$

A typical relationship between C_p and λ is shown in Fig. 2. It is clear from this figure that there is a value of λ for which C_p is maximum and that maximize the power

for a given wind speed. The peak power for each wind speed occurs at the point where C_p is maximized. To maximize the generated power, it is therefore desirable for the generator to have a power characteristic that will follow the maximum C_{pmax} line.

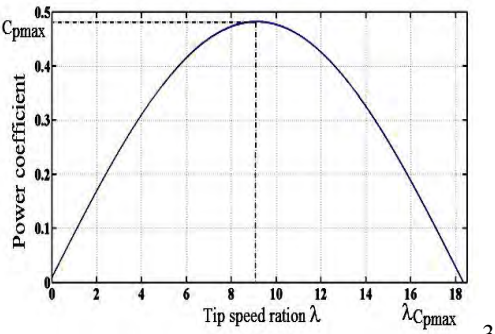

3

Fig. 2: The Power coefficient for the wind turbine model

The action of the speed corrector must achieve two tasks [13]:

- It must control the mechanical speed Ω_{mec} in order to yet a speed reference Ω_{mec_ref}
- It must attenuate the action of the aerodynamic torque, which is an input disturbance.

Taking into account equations (1), (2) and (3), power on the out axle of the turbine is then,

$$P_t = \frac{1}{2} \times C_p \times \rho \times \pi \times R^5 \times \frac{\Omega_t}{\lambda^3} \tag{4}$$

Torque is then,

$$C_t = P_t / \Omega_t \tag{5}$$

$$C_{em} = P_t / \Omega_t = \frac{1}{2} \times \rho \times \pi \times R^3 \times C_p \times v_w^3 \tag{6}$$

With the multiplier of report/ratio G, the torque and speed become at shaft end;

$$C_g = \frac{C_t}{G} \qquad \text{and} \qquad \Omega_t = \frac{\Omega_{mec}}{G} \tag{7}$$

When the turbine is coupled to a machine the mechanical equation at shaft end will be,

$$J \times \frac{d\Omega_{mec}}{dt} + f \times \Omega_{mec} = C_g - C_{em} \tag{8}$$

From these various equations the mathematical model of the turbine at shaft end is shown on Fig. 3.

The expression of the optimal mechanical power P_{mec_opt} is obtained as follows,

$$P_{mec\_opt} = \frac{1}{2} \times \frac{C_{pmax} \times \rho \times \pi \times R^3}{G^3 \times \lambda_{opt}^3} \times \Omega_{mec}^3 \tag{9}$$

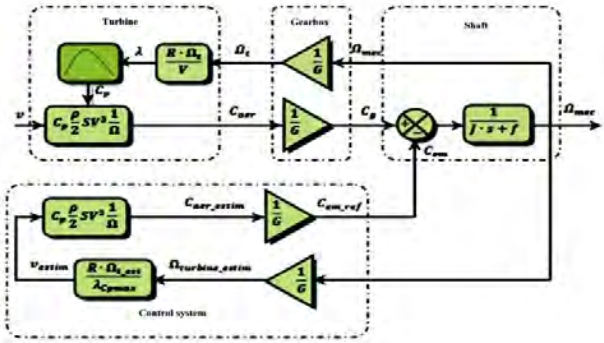

Fig. 3: Device control without control speed, [13]

3. DYNAMICAL MODEL OF THE BDFIG

The electrical equations of the BDFIG in the synchronous reference frame (d-q) are this given by [10]:

$$V_{sp}^{q} = R_{sp} \times i_{p}^{q} + \frac{d\Psi_{sp}^{q}}{dt} + \Psi_{sp}^{d} \times \omega_{p} \tag{10}$$

$$V_{sp}^{d} = R_{sp} \times i_{p}^{d} + \frac{d\Psi_{sp}^{d}}{dt} + \Psi_{sp}^{q} \times \omega_{p} \tag{11}$$

$$0 = R_{r} \times i_{r}^{q} + \frac{d\Psi_{r}^{q}}{dt} + (\omega_{p} - p_{p} \times \omega_{r}) \times \Psi_{r}^{d} \tag{12}$$

$$0 = R_{r} \times i_{r}^{d} + \frac{d\Psi_{r}^{d}}{dt} + (\omega_{p} - p_{p} \times \omega_{r}) \times \Psi_{r}^{q} \tag{13}$$

$$V_{sc}^{q} = R_{sc} \times i_{sc}^{q} + \frac{d\Psi_{sc}^{q}}{dt} + (\omega_{p} - (p_{p} + p_{c}) \times \omega_{c}) \times \Psi_{sc}^{d} \tag{14}$$

$$V_{sc}^{d} = R_{sc} \times i_{sc}^{d} + \frac{d\Psi_{sc}^{d}}{dt} - (\omega_{p} - (p_{p} + p_{c}) \times \omega_{c}) \times \Psi_{sc}^{q} \tag{15}$$

The expressions for stator and rotor flux linkages are,

$$\Psi_{sp}^{q} = L_{sp} \times i_{sp}^{q} + L_{mp} \times i_{r}^{q} \tag{16}$$

$$\Psi_{sp}^{d} = L_{sp} \times i_{sp}^{d} + L_{mp} \times i_{r}^{d} \tag{17}$$

$$\Psi_{r}^{q} = L_{mp} \times i_{sp}^{q} + L_{r} \times i_{r}^{q} + L_{mc} \times i_{sc}^{q} \tag{18}$$

$$\Psi_{r}^{d} = L_{mp} \times i_{sp}^{d} + L_{r} \times i_{r}^{d} + L_{mc} \times i_{sc}^{d} \tag{19}$$

$$\Psi_{sc}^{q} = L_{sc} \times i_{sc}^{q} + L_{mc} \times i_{r}^{q} \tag{20}$$

$$\Psi_{sc}^{d} = L_{sc} \times i_{sc}^{d} + L_{mc} \times i_{r}^{d} \tag{21}$$

The dynamic equations in (10-21) are usually represented in the selected $d-q$ reference frame. The appropriate frame diagrams for the PW are shown in Fig. 4, in which D_c and Q_c are the d, q axes of selected frame and rotate with the synchronous speed ω_e. Fig. 4b- shows the relation of rotor frame with selected reference frame, where the rotor frame revolves at the rotor mechanical speed ω_r. For the CW, the rotor frame would be same as PW due to the back-to-back connection. But the stator frame rotates at the speed ωc, which is shown in Fig. 5. Moreover; Fig. 5 also shows the angle relationship of power machine stator, PW and CW rotors and CW stator to the selected reference frame.

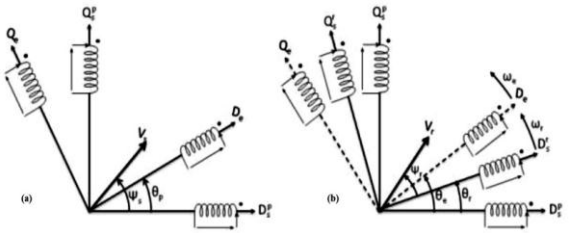

Fig. 4: PW reference D-Q frames: (a) stator and (b) rotor

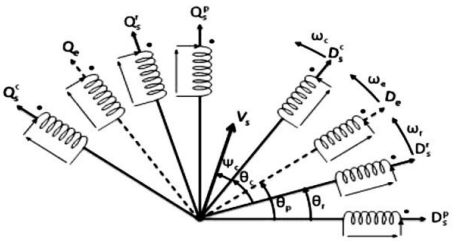

Fig. 5: Control winging reference D-Q frame

The general relationships between these quantities as well as the electrical speed of the rotor for the 50 Hz system are,

$$\begin{cases} \omega_p = 2\pi \times 50 \\ \omega_r = \omega_p - \omega_m \times P_p \\ \omega_r = \omega_p - \omega_m \times (P_p + P_c) \end{cases} \quad (22)$$

The equation also shows the torque to be the function of the PW flux as well as the CW stator and rotor currents,

$$T_{em} = \frac{3}{2} \times \left(P_p (\Psi_{sp}^d \times I_{sp}^d - \Psi_{sp}^q \times I_{sp}^q) + p_c \times L_{mc} (I_{sc}^d \times I_r^q - I_{sc}^q \times I_r^d) \right) \quad (23)$$

Finally, the mechanical model of BDFIG can be written as,

$$J_g \times \frac{d\omega_m}{dt} = T_{em} - F_g \times \omega_m - T_L \quad (24)$$

4. BDFIG CONTROLLER DESIGN

4.1 Control of the grid inverter

The various control strategies for the VSR have been proposed [14] and will be briefly discussed here.

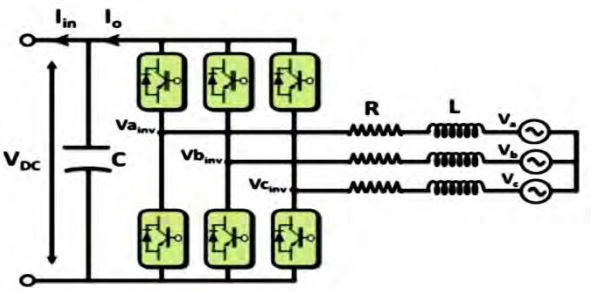

Fig. 6: VSR circuit model

The objective of the grid inverter is to maintain a constant DC-link voltage for between CW and grid. The block diagram of the converter with its controllers [14, 15] is presented in Fig. 6.

The system can be described by the following equation:

$$\begin{bmatrix} V_a \\ V_b \\ V_c \end{bmatrix} = R \times \begin{bmatrix} i_a \\ i_b \\ i_c \end{bmatrix} + L \frac{d}{dt} \begin{bmatrix} i_a \\ i_b \\ i_c \end{bmatrix} + \begin{bmatrix} V_{a_{inv}} \\ V_{b_{inv}} \\ V_{c_{inv}} \end{bmatrix} \tag{25}$$

This can be written in a rotating reference frame by using Park transformation

$$\begin{bmatrix} V_q \\ V_d \end{bmatrix} = R \times \begin{bmatrix} I_q \\ I_d \end{bmatrix} + s \times L \times \begin{bmatrix} I_q \\ I_d \end{bmatrix} + \omega_e \times L \begin{bmatrix} I_q \\ -I_d \end{bmatrix} + \begin{bmatrix} V_{q_{inv}} \\ V_{d_{inv}} \end{bmatrix} \tag{26}$$

$$\begin{aligned} P &= \frac{3}{2} \times (V_d \times I_d + V_q \times I_q) \\ Q &= \frac{3}{2} \times (V_q \times I_d + V_d \times I_q) \end{aligned} \tag{27}$$

The direct axis current is used to regulate the reactive power and the quadrature axis current is used to regulate the DC-link voltage. The reference frame is considered oriented along the stator voltage vector. This method gives possibility to make independent control of the active and reactive powers between the front end converter and the supply side. The voltage components in the Park frame V_{d_inv} and V_{q_inv} are given at the output of the PI regulator:

$$\begin{aligned} V_d^* &= -I_d \times (L_s + R) + (\omega_e \times L \times I_q + V_d) \\ V_q^* &= -I_q \times (L_s + R) + (\omega_e \times L \times I_d) \end{aligned} \tag{28}$$

In the Park reference frame, the voltage source components are $V_d = 0$ and $V_q = V_s$ and the powers can be written as,

$$P = \frac{3}{2} \times V_q \times I_q \quad \text{and} \quad Q = \frac{3}{2} \times V_q \times I_d \tag{29}$$

By neglecting the converter losses, we have,

$$V_{dc} \times I_{dc} = \frac{3}{2} \times V_q \times I_q \quad \text{and} \quad C \times \frac{dV_{dc}}{dt} = I_{in} - I_0 \tag{30}$$

$$V_{dc} \times C \times \frac{d V_{dc}}{d t} = P - P_m \tag{31}$$

The inner current loop can be modeled as a transfer function relating the terminal voltage and current:

$$\frac{I(s)}{V(s)} = \frac{1}{L_s + R} \tag{32}$$

The complete block diagram of the VSR controller is shown in Fig. 8.

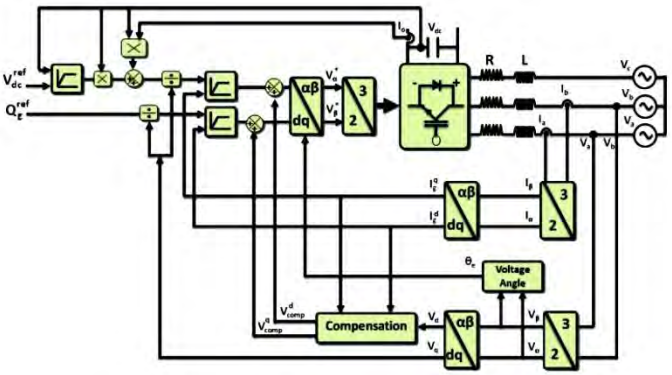

Fig. 7: Grid side VSR

4.2 Machine side controller

The developed control strategy is based on a loops control as shown in Fig. 8. Two regulation paths are implemented as in the classical vector control schemes: one control path regulates the d magnetizing currents and the other one is dedicated to control the q active currents.

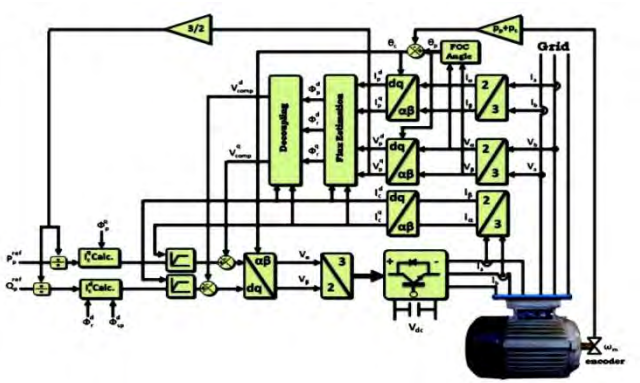

Fig. 8: Block diagram of BDFM power control system

In order to obtain a good decoupled control, the power machine flux orientation has been selected ($\Psi_{sp}^{d} = \left|\Psi_{sp}\right|$ and $\Psi_{sp}^{q} = 0$). The obtained control strategy for the BDFM is similar to the well-known stator field orientation control used in the DFIM. [6, 11].

5. PID CONTROLLER SYNTHESIS

At present, the PID-type controller is most widely adopted in industrial application due to its simple structure, as shown Fig. 9. Its control signal is easily computed by combining proportional-integral-Derivative terms, weighted according to the independent gain parameters P, I, and D [16]. The filter coefficient N sets the location of the pole in the derivative filter. The control signal is,

$$u(t) = \left(K_p + K_i \times \left(\frac{1}{s} \right) + K_d \left(\frac{N \times s}{s + N} \right) \right) \times e(t) \tag{33}$$

The terms K_p, K_i and K_d represent respectively the proportional, integral and derivative gains.

The quotient B / A represents the transfer function to be controlled, where A and B are presently defined as follows:

$$A = R_{sc} + s\delta_3 \quad \text{and} \quad B = 1 \tag{34}$$

Where,

$$\delta_3 = L_{sc} - \frac{L_{mc}^2 \times L_{sp}}{L_r \times L_{sp} - L_{mp}^2} \tag{35}$$

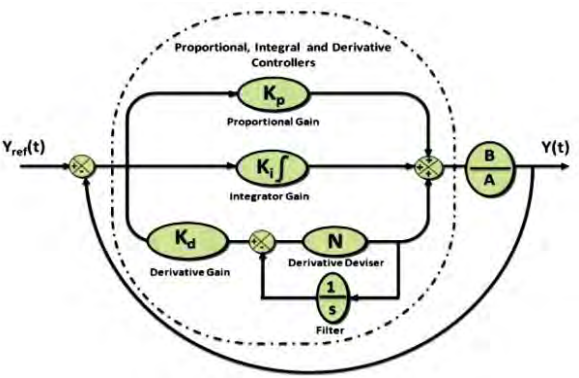

Fig. 8: System with PID controller

The controller terms can be calculated just specifying the natural frequency and damping of the close loop equivalent second order system. The desired natural frequency (ω_n) and damping (ξ) are set respectively to 37 rad/s and 70.7 %.

Allows determining the parameters of PID controller:

$K_p = 1.84$, $K_i = 62$ and $K_d = -0.015$ and $N = 123$.

6. PERFORMANCES OF THE CONTROLLER

The aim of the control is to have measured active and reactive powers equal to the reference values. These powers must then be collected.

In order to measure only the stator current of CW. The PID controller has been tested using the indirect control method. The indirect control mode is based on the stator currents measurements of CW.

6.1 Reference tracking

The first test investigated to compare the tow controllers is reference tracking by applying stator active and reactive power steps to the BDFIG, while the machine's speed is maintained constant at 75 rd/s corresponds to 716.5 rpm. The BDFIG is considered as working over ideal conditions (no perturbations and no parameters variations), The results are presented in Fig. 10.

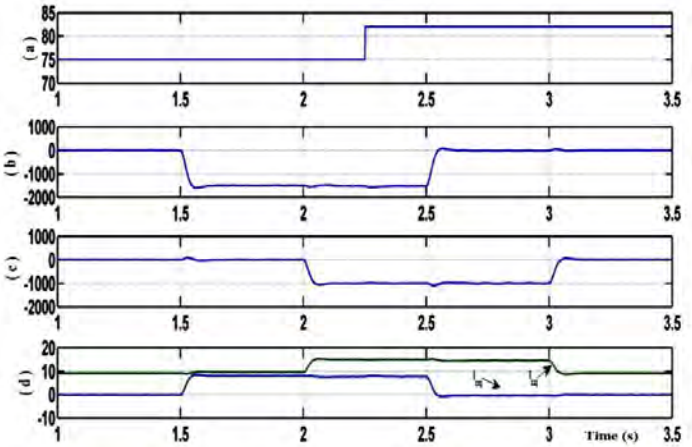

Fig. 10: Simulated results under various speed and stator reactive power steps

(a) Rotor speed (rd/s), **(b)** Stator active power of PW (W)
(c) Reactive power of PW (Var), **(d)** Direct and quadratic stator currents of CW (A)

6.2 Simulation of the whole system

The brushless doubly fed induction generator parameters used in the simulation are given as following.

Table 2: BDFIG parameters used for simulation

Turbine	
	Diameter = 4.6 m, Number of blades = 3, Hub height = 12 m, Gearbox = 18
BDFIG	
	2.5 kW, 380 V, 50 Hz, 2 pole pairs, R_{sp} = 1.732 Ω, R_{sc} = 1.079 Ω, R_r = 0.473Ω, L_{sp} = 714.8 mH, L_{sc} = 121.7 mH, L_r = 132.6 mH.
Grid	
	$U = 380\,V$, $Z_{line} = R + j\,L\omega = 0.25 + j0.003$

Fig. 11 shows the angular speed random of the BDFIG. Fig. 12 presents the wind generator mechanical power. The decoupling effect of the between the direct and quadratic stator flux of PW is illustrated in Fig. 13.

The stator currents and voltages waveforms of the BDFIG and the related expended plots are shown, respectively, in Fig. 14a-, Fig. 14b-, Fig. 14c- and Fig. 14d- (phase α). The PWM inverters are operated at 2 kHz; hence, the currents are almost sinusoidal.

The stator currents (PW and CW) waveforms and these zoom are presented, correspondingly, in Fig. 15a- and Fig. 15b-. Fig. 16 gives the rotor current of the BDFIG.

The grid voltage and current waveforms and these zoom are presented, correspondingly, in Fig. 17a- and Fig. 17b-. The stator active and reactive powers are plotted in Fig. 18. Fig. 19a- and Fig. 19b- show the regulation of the DC-link voltage.

It is maintained at a constant level (410 V) so that the real power extracted from the wind energy conversion system can pass through the grid.

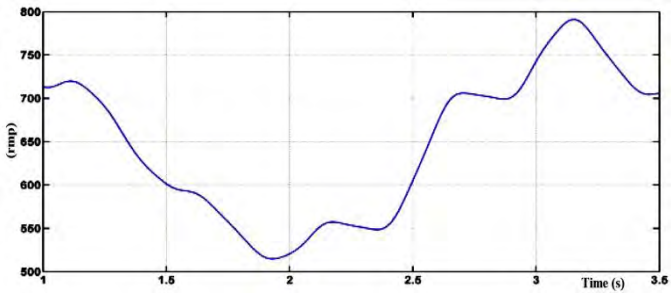

Fig. 11: Random of the BDFIG rotor speed (Ω_{mec})

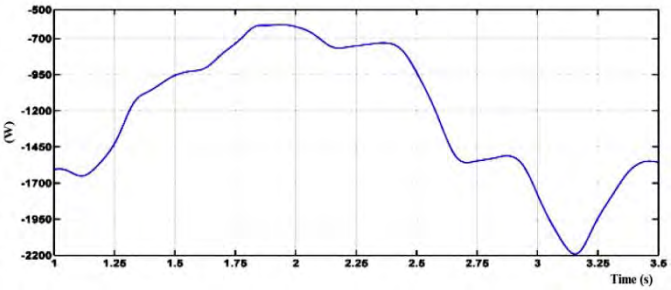

Fig. 12: Wind generator mechanical power (P_{mec})

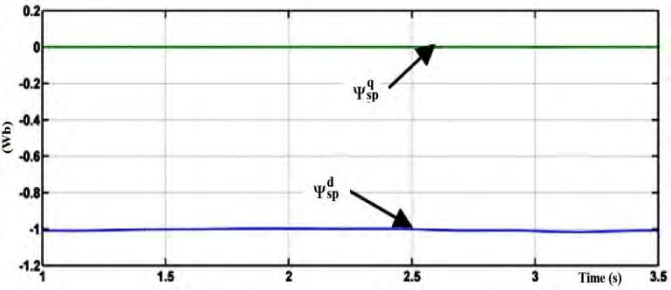

Fig. 13: Direct and quadratic stator flux of PW (Ψ_{sp}^{q} and Ψ_{sp}^{d})

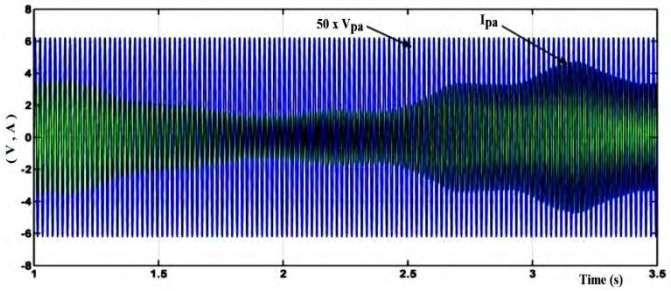

Fig. 14a: Stator current and voltage of PW (I_{sp}^{a} , V_{sp}^{a})

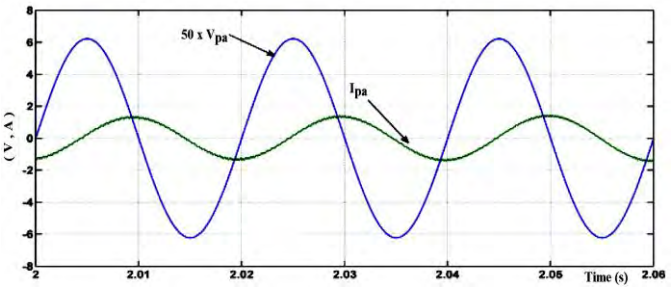

Fig. 14b: Zoom of stator current and voltage of PW (I_{sp}^{a} , V_{sp}^{a})

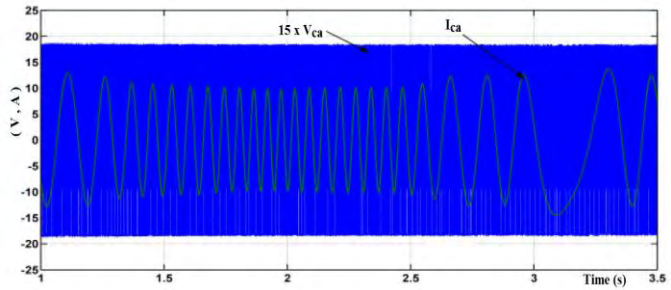

Fig. 14c: Stator current and voltage of CW (I_{sc}^{a} , V_{sc}^{a})

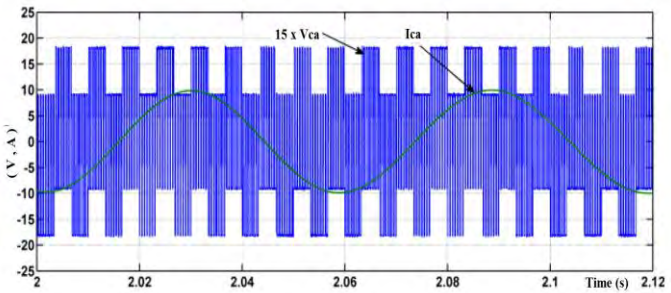

Fig. 14d: Zoom of stator current and voltage of CW (I_{sc}^{a} , V_{sc}^{a})

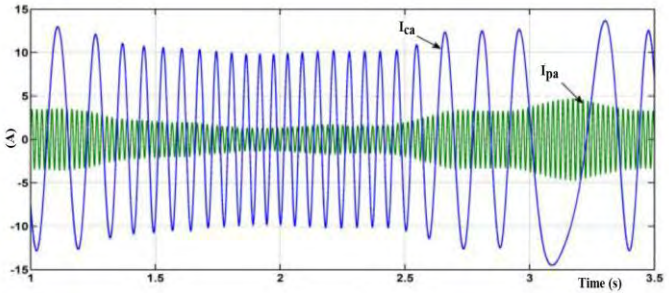

Fig. 15a: Stator currents of PW and CW (I_{sc}^{a} , I_{sc}^{a})

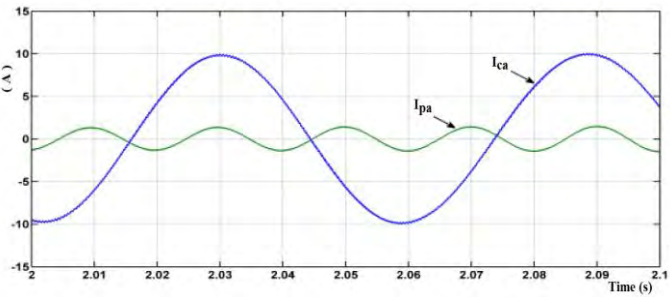

Fig. 15b: Zoom of stator currents of PW and CW (I_{sc}^{a} , I_{sc}^{a})

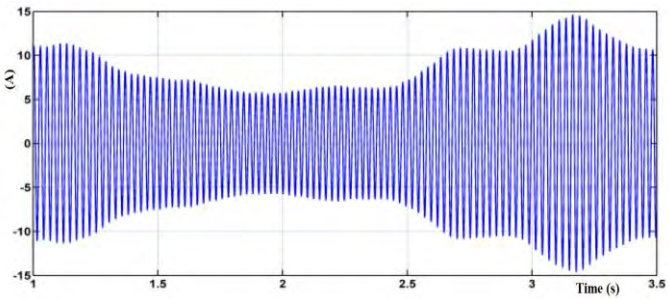

Fig. 16: Rotor current (I_{r}^{a})

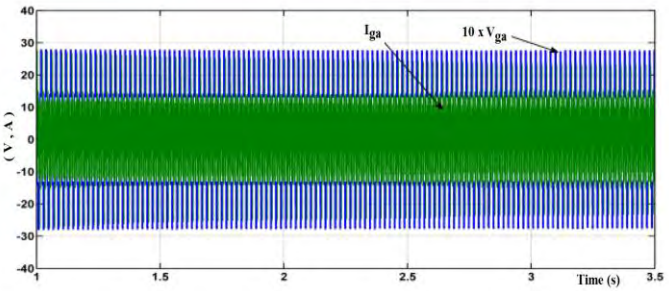

Fig. 17a: Grid voltage and current (I_{g}^{a} , V_{g}^{a})

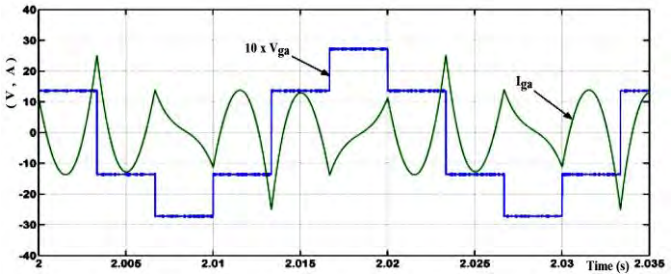

Fig. 17b: Zoom of grid voltage and current (I_g^a , V_g^a)

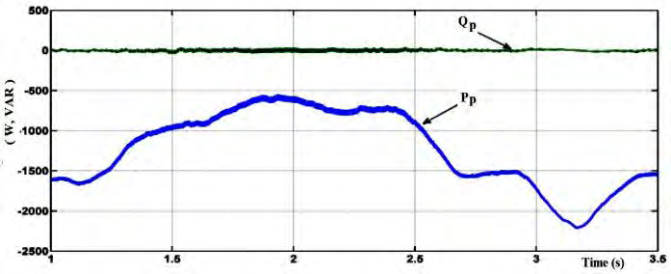

Fig. 18: Stator active and reactive powers (P_p , Q_p)

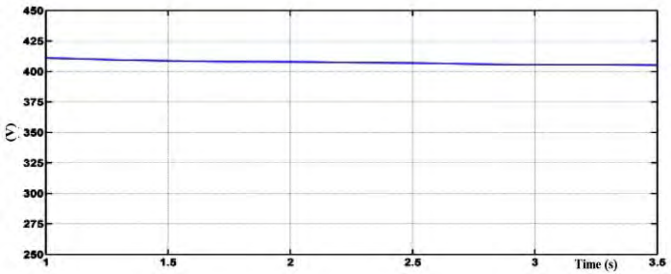

Fig. 19a: DC-link voltage (E)

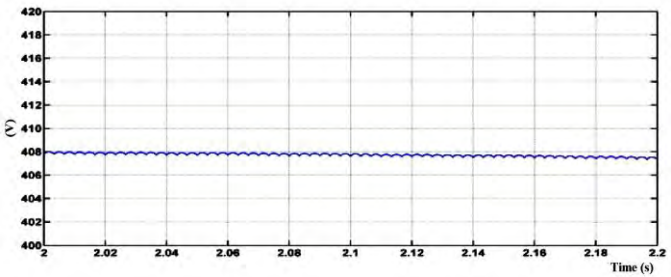

Fig. 19b: Zoom of DC-link voltage (E)

7. CONCLUSION

Owing to its great reliability, BDFIG is an interesting solution for wind energy applications. It has been also shown in this paper that using an appropriate modeling approach based on dynamical equivalent circuit representation; a theoretical and

simulation study of the BDFIG dynamic performance in closed loop control of the generator active and reactive powers has been presented.

The control system is based on the field orientation principle and the orientation of the power machine stator flux with two PID controllers placed in the power stator field coordinates, where a back-to-back voltage source converter was employed. Moreover, the proposed modeling approach allows the study of power flow.

The effectiveness of the proposed controllers has been demonstrated by simulation and successfully implemented in a wind driven brushless doubly fed induction generator system.

APPENDIX A. NOMENCLATURE

Turbine	
Ω_{mec}: Mechanical speed of the BDFIG	P_t : Mechanical power
Ω_t: Turbine speed	P_{mec_ref} : Mechanical power optimal
Ω_{mec_ref}: Mechanical speed reference	C_{aer}: Aerodynamic torque
C_g: Generator torque	ρ: Air density
C_p: Power coefficient	R: Turbine radius
λ :Tip speed ratio	V_w : Wind velocity
G: Gear ratio	J_t: Inertia
S: Cross-sectional area	F_t Viscous friction
BDFIG	
$V_{sp}^q, V_{sp}^d, V_{sc}^q, V_{sc}^d$: "d-q" stators voltages	$\psi_{sp}^q, \psi_{sp}^d, \psi_{sc}^q, \psi_{sc}^d$: "d-q" stators flux
$i_{sp}^q, i_{sp}^d, i_{sc}^q, i_{sc}^d$: "d-q" stators currents	V_r^q, V_r^d: "d-q" rotor voltages
i_r^q, i_r^d: "d-q" rotor currents	R_r : Per phase rotor resistance
R_{sp}, R_{sc}: Per phase stators resistances	L_{sp}, L_{sc}: Total cyclic stators inductances
L_r: Total cyclic rotor inductance	p: Number of pole pairs
L_{mp}, L_{mc}: Magnetizing inductances	s: Derivative operator
J_g: Inertia	C_{em}: Electromagnetic torque
Fg: Viscous friction	P_p, Q_p: Active and reactive stator powers
P_g, Q_g: Active and reactive grid powers	ω_e: Speed of the reference frame
ω_p, ω_c: Stators synchronous angular frequency	ω_r: Rotor's electrical angular speed

REFERENCE

[1] S. Muller, M. Deicke and R.W. De Doncker, '*Doubly Fed Induction Generator Systems for Wind Turbines*', IEEE Industry Applications Magazine, Vol. 8, N°3, pp. 26 – 33, 2002.

[2] F. Runcos, R. Carlson, A. Oliveira, P. Kuo-Pen and N. Sadowski, '*Performance Analysis of a Brushless Double Fed Cage Induction Generator*', Proceedings Nordic Wind Power Conference, pp. 1 – 8, 2004.

[3] N. Chilakapati, V.S. Ramsden and V. Ramaswamy, '*Performance Evaluation of Doubly-Fed Twin Stator Induction Machine Drive With Voltage and Current Space Vector Control Schemes*', IEE Proceedings Electrial Power Applications, Vol. 148, N°3, pp. 287 – 292, 2001.

[4] W. Grainger and N. Jenkins, '*Offshore Wind Farm Electrical Connection Options*', Offshore Wind Energy Network [Online]. Available: www.owen.eru.rl.ac.uk

[5] F. Blaschke, '*The Principle of Field Orientation as Applied to the New Transvector Closed-Loop Control System for Rotating Field Machines*', Siemens Review, N°2, pp: 217 – 223, 1972.

[6] J. Poza, E. Oyarbide, I. Sarasola and M. Rodriguez, '*Vector Control Design and Experimental Evaluation for the Brushless Doubly Fed Machine*', IET Electric Power Applications, Vol. 3, N°4, pp. 247 –256, 2009.

[7] N. Patin, E. Monmasson and J.P. Louis, '*Modeling and Control of a Cascaded Doubly Fed Induction Generator Dedicated to Isolated Grids*', IEEE Transactions Industrial Electronics, Vol. 56, N°10, pp. 4207 – 4219, 2009.

[8] N. Patin, '*Analyse d'Architectures, Modélisation et Commande de Générateurs pour Réseaux Autonomes*', Thèse de Doctorat, Ecole Normale Supérieure de Cachan. 2006.

[9] Sh. Shao, E. Abdi, F. Barati and R.A. McMahon, '*Stator-Flux Oriented Vector Control for Brushless Doubly Fed Induction Generator*', IEEE Transactions on Industrial Electronics, Vol. 56, N°10, pp. 4220 - 4228, 2009.

[10] J. Poza, E. Oyarbide, I. Sarasola and M. Rodriguez, '*Unified Reference Frame d-q Model of the Brushless Doubly Fed Machine*', IEE Proceedings Electric Power Applications, Vol. 153, N°5, pp. 726 - 734, Sep. 2006.

[11] I. Sarasola, J. Poza, M.A. Rodriguez and G. Abad, '*Direct Torque Control Design and Experimental Evaluation for the Brushless Doubly Fed Machine*', Energy Conversion and Management, Vol. 52, N°2, pp. 1226 – 1234, 2011.

[12] I. Sarasola Altuna, '*Control Robusto de Una Máquina de Inducción Doblemente Alimentada por el Estator en Aplicaciones de Generación de Energía a Velocidad Variable*', Mondragón Goi Eskola Politeknikoa, Spain, 2008.

[13] S. El Aimani, '*Modelling and Simulation of Doubly Fed Induction Generator for Variable Speed Wind Turbines Integrated in a Distribution Network*', In: 10th European Conference on Power Electronics and Application, Toulouse, France, 2003.

[14] K. Protsenko and D. Xu, '*Modeling and Control of Brushless Doubly-Fed Induction Generators in Wind Energy Applications*', Applied Power Electronics Conference and Exposition Annual IEEE Conference, APEC, pp. 529 - 535, 2007.

[15] R. Pena, J.C. Clare and G.M. Asher, '*Doubly Fed Induction Generator Using Back-To-Back PWM Converters and its Application to Variable Speed Wind-Energy Generation*', IEE Proceedings Electric Power Applications, Vol. 143, N°3, pp. 231 – 241, 1996.

[16] K. Astrom and T. Hagglund, '*PID Controllers: Theory, Design, and Tuning*', Instrument Society of America, 1995.